RAD Conference Proceedings, vol. 9, pp. 1-6, 2025
ISSN 2466-4626 (online) | DOI: 10.21175/RadProc.2025.1
www.rad-proceedings.org

ADVANCED DIGITAL IMAGE PROCESSING FOR MATERIAL EVALUATION IN NUCLEAR APPLICATIONS

Ondřej Pašta[1*], Jaroslav Knotek[1], Jan Blažek[2], Marcin Kopeć[1]

[1]Research Centre Řež s.r.o., Hlavní 130, Řež, 250 68 Husinec, Czech Republic
[2]Institute of Information Theory and Automation of the CAS v.v.i., Pod Vodárenskou věží 1143/4, 182 00, Prague 8, Czech Republic

Abstract. *The integration of digital image processing (DIP), neural networks, and artificial intelligence (AI) is transforming materials science by enabling automated, high-resolution analysis of microscopic structures and supporting applications across nuclear research. At Research Centre Řež (CVR), DIP and AI have improved efficiency and reproducibility in workflows such as the classification of microstructural precipitates—both manufacturing-related secondary phase particles and radiation-induced precipitates—whose morphology and distribution affect key mechanical properties. These methods are also applied to the structural assessment of biological shielding concrete, where DIP detects and quantifies crack development, complementing traditional non-destructive testing. In fuel inspections and post-irradiation examinations, DIP enhances video analysis and microscopy, reducing manual bias while ensuring consistent evaluation of cladding and structural components. Overall, DIP technologies developed at CVR strengthen long-term operation (LTO) strategies in nuclear energy and offer versatile solutions for other sectors requiring precise microstructural or surface characterization.*

Keywords: *material science, data analysis, PIE, precipitates, biological shielding, cladding, nuclear fuel*

1. INTRODUCTION

The safe and reliable operation of nuclear power plants (NPPs) is a cornerstone of global energy infrastructure. As the global fleet of reactors ages, there is increasing interest in extending their operational life beyond the original 30–40 years up to 60, 80, or even 100 years. Long-term operation (LTO) strategies have therefore become a priority for both industry and the research community [1], [2]. This effort requires accurate diagnostics of aging phenomena in components exposed to extreme environments of thermal, mechanical, and radiation-induced stress [1], [3], [4].

Among the key structural elements requiring close monitoring is the biological shielding, commonly made of concrete. Its integrity is vital for protecting personnel and sensitive systems from neutron and gamma radiation. However, its long-term performance is challenged by radiation-induced volumetric expansion (RIVE) in quartz aggregates and chemical degradation due to water radiolysis. These effects lead to microcrack formation, compromising stiffness, strength, and shielding capacity [5], [6].

Another focus of LTO diagnostics is the reactor pressure vessel (RPV) and its internals, including fuel cladding and fuel assemblies. These materials are affected by neutron flux, temperature gradients, and mechanical loads, which alter their microstructure—especially through the formation of secondary phase particles (SPPs) and radiation-induced precipitates (RIPs). These features impact mechanical properties such as fracture resistance and hardness [7].

All components can be subjected to reactor conditions—neutron fluence >1×10^{19} n/cm^2, gamma doses up to 300 MGy, and temperatures exceeding 90°C [1], [2].

Recent advances in Digital Image Processing (DIP) and Artificial Intelligence (AI) have enabled precise, high-throughput analysis of structural degradation. At Research Centre Řež (CVR), DIP has been integrated into inspection workflows involving Scanning Electron Microscopy/Transmission Electron Microscopy (SEM/TEM), visual fuel inspections, and concrete cracking studies. These methods enhance Post-Irradiation Examinations (PIE) by providing objective, reproducible, and quantitative insights [8], [9].

This paper presents the application of DIP in three nuclear material domains at CVR: (1) inspection of fuel assemblies, (2) microcrack detection in shielding concrete, and (3) precipitate characterization in cladding materials. Together, these demonstrate how DIP enables improved diagnostics for LTO support.

* E-mail of the corresponding author – ondrej.pasta@cvrez.cz

2. Materials and Methods

This study is based on experiments and inspections conducted at CVR, where DIP and AI tools have been integrated across nuclear research domains. The analysed materials included fuel assemblies and claddings, biological shielding concrete, and irradiated structural alloys.

Automated DIP workflows were developed using Python and MATLAB, integrated with OpenCV, scikit-image, and TensorFlow [10], [11], [12]. These tools enabled rapid image labeling, neural network training, and batch processing of terabyte-scale image datasets. All results were cross-validated with conventional methods (e.g., ultrasonic testing, profilometry) for consistency. In concrete studies, DIP-derived crack data were correlated with mechanical parameters like compressive strength, Young modul, and porosity.

The micrography images were obtained with the use of Tescan Lyra3 and Tescan Mira3 microscopes. Although the TEM activities are still at their beginning, the initial images were obtained with the use of Jeol jem 2200fs.

The work foreseen different enhancements of the microscopes to improve the robustness of the whole system. In this way, for the SEM micrography, there were used the enhancements of: 10, 40, and 250 μm viewfield.

2.1. Shielding Concrete: RIVE and Cracking

Test specimens reflected historical compositions of Water-Water Energetic Reactor (VVER) shielding concrete, emphasizing quartz-rich aggregates prone to RIVE. Cracking was evaluated under controlled thermal and irradiation loads using high-resolution imaging and DIP. DIP enabled quantification of microcrack initiation, propagation, and deformation fields in 2D and 3D spaces [5].

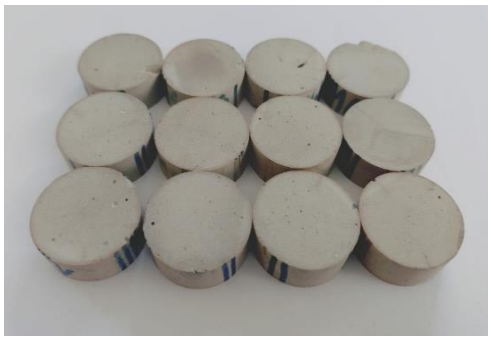

Figure 1. Concrete shielding samples.

2.2. Fuel Cladding: Microstructural Evolution

To assess irradiation-induced microstructural changes in cladding alloys, SEM and TEM imaging were conducted. DIP algorithms performed image segmentation and particle analysis—extracting data on precipitate morphology, size, and distribution. These workflows included contrast enhancement, noise filtering, thresholding, and segmentation via neural networks trained on annotated datasets [6], [7].

2.3. Fuel Assemblies: Geometric Verification

The specimens of the fuel rod deformations—such as bowing, twisting, and axial growth—were evaluated using DIP on hot cell investigation videos. These were processed into high-resolution 2D and pseudo-3D composites with ~0.2 mm spatial resolution, allowing for cycle-to-cycle dimensional tracking under LTO scenarios [8].

To assess creep behavior, small cladding specimens were tested within hot cells. Using nanoindentation, a reference grid was imprinted and optically tracked using tools such as Vertex. Initial measurements were followed by irradiation under reactor-relevant conditions and post-irradiation re-measurement of each grid point [13], [14], [15]. This enabled precise quantification of deformation under LTO-relevant stresses.

3. Results and Discussion

During reactor operation, fuel rods undergo deformation due to thermal loads, hydraulic forces, and irradiation-induced swelling [16]. Traditional inspections often rely on manual visual assessments—susceptible to subjectivity and limited in resolution [17]. DIP has enabled automated, high-resolution image reconstruction for fuel rod evaluation, achieving sub-millimeter accuracy [18], [19], [20].

Video frames are stabilized, denoised, and stitched into continuous composites. Using CNN-based feature detection, geometric anomalies are tracked longitudinally. This has been historically implemented at CVR for routine fuel inspections, supporting licensing, design optimization, and PIE.

The first step in cladding samples evaluation after PIE data processing is image cleaning. To suppress low-frequency background variations, grayscale morphological erosion is applied and subtracted from the original image. Next, small surface scratches—typically smaller than the indents—are removed using a grayscale morphological "opening" operation with a kernel size of 9 pixels. Once cleaned, the image is thresholded using a predefined value of 70 to isolate high-intensity regions.

Following thresholding, individual components in the image—continuous white regions—are identified. These components are then connected to their neighbors using Delaunay triangulation, forming a graph that maps potential neighboring relationships. However, this graph often includes a significant number of incorrectly identified indents, as well as invalid neighbor connections, such as diagonal edges or connections to noise-related artefacts. To address this, false edges and nodes are filtered out based on the regularity of the nanoindentation grid (see Figure 2).

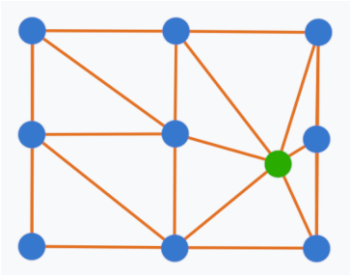

Figure 2: Delaunay triangulation of image components' centroids (blue nanoindentation, green anomaly). A component is considered an anomaly if it does not fit into the grid pattern.

Due to image defects and the subsequent filtering process, some valid indents may be unintentionally lost. If the number of missing indentations is small, the grid can still be completed through interpolation. However, if the grid cannot be reconstructed properly or critical points are missing, the algorithm prompts the user to perform a manual inspection and correction.

Concrete exposed to high radiation undergoes RIVE, microcracking, and chemical degradation [7]. At CVR, DIP and DIC methods have been applied to visualize crack propagation and quantify strain localization at quartz-cement interfaces. Observations align with ICIC findings, confirming the importance of high-resolution, localized imaging.

Detecting cracks in sample materials can be challenging and often requires expert-level interpretation. In light of this, a manual annotation of cracks on randomly selected video frames was carried out. A dataset was created consisting of approximately one hundred annotated frames, each labelled independently by three different experts. These annotations serve multiple purposes: they allow for cross-validation between individual annotators, enable training of machine learning models for crack detection, and support the validation of automated detection tools.

The annotated cracks represent damage that spans the entire volume of the sample, making them suitable for visual analysis and assessment. To characterize this damage as accurately as possible, we focus on extracting a set of descriptive parameters from the segmented cracks. These parameters are inspired by widely adopted evaluation metrics and were implemented in our own software tool developed specifically for crack assessment.

For each evaluated sample, the following set of measurements is computed. First, the total number of cracks is determined. Then, for each individual crack, its length in pixels, its size in pixels (accounting for both length and width), the maximum and average width, the perimeter of the crack in pixels, and the distance between its two most distant pixels are calculated. The resulting vectors of these values are used to assess the extent of damage in the sample.

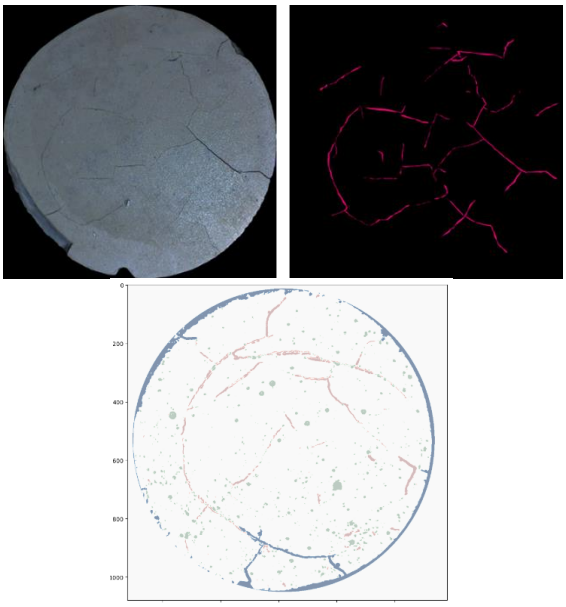

Figure 3. Original image of the sample after scanning and cracking registration (above), aggregated outputs of all findings after processing a single batch of concrete samples (below).

As shown in the Figure 3 above, the DIP system tracks the crack pattern in each frame of the video. Then, it aggregates the photos and the resulting crack recognition into a single photo sample and crack mapping. Along with this process, there is a need to extract noise coming from the porous structure of the sample and the missing parts within the rim area of the sample. In this way, a final cracking map is produced, and the data can be crossed with the Ultrasonic Testing (UT) measurement (see Figure 4) and physical changes of the sample (geometrical and mass changes).

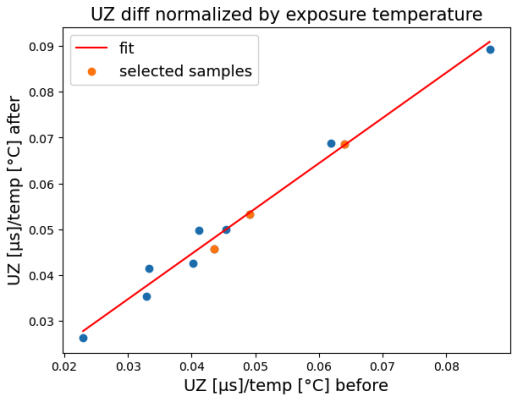

Figure 4. Obtained UT measurements results normalized by the exposition temperature (constant time).

DIP results also showed high correlation with ultrasonic and acoustic NDT data, validating its use in structural integrity assessments of reactor shielding. The thermal ageing of the concrete samples, which reveals itself in cracking formation, is clearly shown in Figure 4. The picture shows matching images of the sample (clearly identified

with the pore pattern) in before- and after—exposition state. The formation of the cracks is directly distinguishable and confirms the expected increase in time of the ultrasonic wave to penetrate the samples.

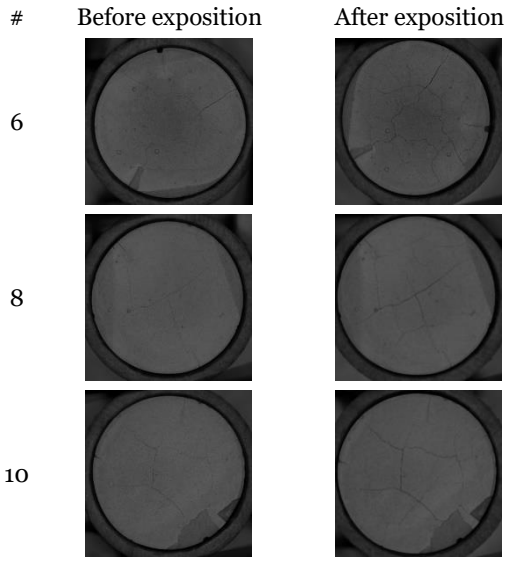

Figure 5. The visual assessment of the three selected samples before and after the thermal exposure according to Figure 3.

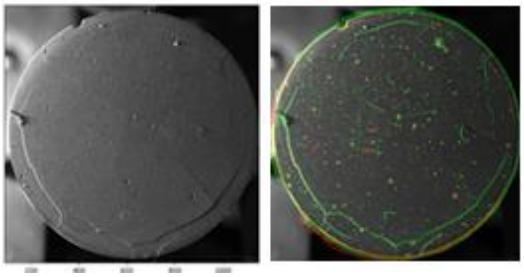

Figure 6. Original registered image (left) and processed outputs of crack, pores, and scratches detection in the binary system (right).

In Figure 6 there are shown the processing outputs of a single concrete sample. The cracking area aggregated into pixels has grown on exposed samples by 40 times when compared to unexposed samples. The aggregated length of the cracks shows by 5 times growth, like the width of the cracks. The cracks ends´ distance has grown by 4 times.

As the scanning equipment is still under development, the amount of valid data is limited and will grow constantly during the application process of the scanner.

Microstructural stability of fuel cladding is critical for mechanical performance. At CVR, DIP-assisted analysis of SEM/TEM images provided detailed quantification of SPPs and RIPs. Parameters like shape, size, and inter-particle distances were statistically analyzed.

The evaluation procedure was conducted using three types of datasets. The primary dataset was a labeled test set, which served as the basis for the quantitative evaluation of model performance. In addition, two auxiliary datasets were used: a portion of the training data excluded due to unreliable labeling, and a set of remaining unlabeled data. Both datasets were used solely for visual validation of the model outputs.

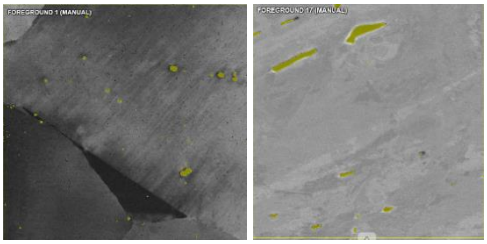

Figure 4. Automatic evaluation of precipitates using an algorithm.

For each image in the datasets, a dedicated folder was generated containing several supporting files. These included the original input image (Img.png), the unthresholded prediction output from the model (Prediction_continuous.png), a CSV file detailing the properties of each detected particle (Precipitates.csv), a visual representation of the identified particles on the input image (Plot_visualized.png), and a histogram showing the size distribution of particles in either micrometers or pixels (Histogram_[µm/px].png).

Model performance was evaluated using the labelled test set, while the other two datasets served for visual inspection only. The predictions were thresholded at a value of 0.5, and the model results were averaged across the entire test set. During hyperparameter optimization, comparable results were achieved using different configurations. The three configurations with the highest F1 scores were selected and are detailed below in the table.

Table 1. Summarization of the average precision, recall, and F1 score achieved by each configuration.

Configuration	Precision	Recall	F1 Score
I	0.838	0.797	0.817
II	0.846	0.788	0.816
III	0.808	0.816	0.812

All three configurations performed comparably, with average F1 scores exceeding 0.81. Configuration I achieved the highest F1 score overall, driven by a balance between strong precision and recall. Configuration II achieved the highest precision but had slightly lower recall. In contrast, configuration III had the highest recall among the three, suggesting it identified more true positives but at the cost of slightly reduced precision.

An additional experiment explored the impact of removing poorly labelled data from the training set. The results supported the hypothesis that excluding such data improves model performance. Specifically,

the exclusion of low-quality labels led to an increase of approximately one to two percentage points in the F1 score, indicating a measurable benefit in overall predictive reliability.

Additionally, in parallel there an experiment was conducted to compare the labelers and the model and to verify the consistency between them. Taking into account that the labeler provides average ground truth of what is actually available to recognize, the derived discrepancies actually show the precision of the model. The data are summarized below in the table on a selection of five photo-samples, typically difficult both for the human operator and the model, for the experiment to be carried out at once, without any disturbance that could influence the labelers. The results combine the F1 parameter and Intersection Over Union (IoU).

Table 2. Comparison between the model and the min/max score achieved by the labelers.

Sample number	IoU			F1		
	Min	Max	Model	Min	Max	Model
1	0.823	0.940	0.861	0.914	0.968	0.778
2	0.856	0.913	0.494	0.817	0.962	0.725
3	0.751	0.871	0.800	0.691	0.982	0.518
4	0.337	0.745	0.573	0.168	0.866	0.367
5	0.829	0.955	0.938	0.962	1.000	0.832

Depending on the input photo samples, the model score varies, but on average across all samples within the Research and Development (R&D) project, it reaches over 80% F1 precision with high consistency. In this way, it is possible to produce pre-labelled outputs for the operator to manually improve the final output. In this way, the work optimization in precipitate recognition – being one of the key goals of the R&D project - is achieved.

This data supports mechanical property prediction and feeds into FEM simulations for modeling cladding failure. DIP also improves reproducibility in PIE workflows and complements existing R&D in irradiation material science [9], [13].

3. Conclusion

The integration of Digital Image Processing (DIP) and artificial intelligence (AI) into nuclear materials research has transformed the way diagnostic information is captured, processed, and interpreted at Research Centre Řež (CVR). By enabling precise, scalable, and reproducible analyses across a range of imaging modalities—from optical inspections and electron microscopy to digital image correlation—DIP has established itself as a powerful enabler of long-term operation (LTO) strategies.

Across fuel assembly inspections, shielding concrete assessments, and cladding microstructure evaluations, DIP methods have demonstrated their capacity to improve data quality, reduce human bias, and accelerate inspection cycles. The integration of automated workflows, machine learning models, and advanced image segmentation has allowed CVR to process terabytes of imaging data with a level of efficiency and accuracy unattainable through traditional means. These image-based diagnostics not only support condition-based monitoring and lifetime prediction but also contribute to improved design validation and post-irradiation analysis.

Beyond nuclear applications, the core principles and computational frameworks of DIP are highly transferable to other domains such as civil engineering, aerospace, and metallurgy—fields where structural integrity and material performance are equally critical. As image data volumes and complexity continue to grow, the role of DIP in ensuring the reliability, safety, and performance of engineered systems is set to become even more central.

Looking forward, further development is expected to focus on increasing automation through AI-driven feature recognition, integrating multimodal imaging sources, and scaling systems for near-real-time applications. In this context, DIP stands not only as a valuable research tool but as a foundational technology for the digital transformation of nuclear infrastructure monitoring.

Acknowledgements: *We acknowledge the state support of the Technology Agency of the Czech Republic within the National Competence Centre Programme II, project TN02000012 „Center of Advanced Nuclear Technology II“.*

References

1. J.T. Busby, R.K. Nanstad, R.E. Stoller, Z. Feng, D.J Naus, “Materials Degradation in Light Water Reactors: Life After 60?”, Oak Ridge National Laboratory, 2008. http://doi.org/10.2172/938766
2. L.J. Bond, “Moving Beyond NDE to Proactive Management of Materials Degradation”, *in Proc. ASME Pressure Vessels and Piping Conf. (PVP)*, 2011, pp. 205-214. http://doi.org/10.1115/PVP2010-26174
3. T.S. Byun, D.A. Collins, T.G. Lach, E.L. Carter, “Degradation of impact toughness in cast stainless steels during long-term thermal aging”, *J. Nucl. Mater.*, vol. 542, 152524, 2020. http://doi.org/10.1016/j.jnucmat.2020.152524
4. O.Y. Chernousenko, T.V. Nikulenkova, A.H. Nikulenkov, “Milestones of Implementation of Aging Management for NPP Components”, *Bull. NTU “KhPI”. Ser.: Power & Heat Eng. Proc. Equip.*, vol. 9 (1181), pp. 85–89, 2016. http://doi.org/10.20998/2078-774X.2016.09.12
5. D. Plašienka, J. Knotek, M. Kopeć, M. Malá, J. Blažek, “Measurement of nuclear fuel assembly’s bow from visual inspection’s video record”, *Nucl. Eng. Des.*, vol. 55, no. 4, pp. 1485-1494, 2023. http://doi.org/10.1016/j.net.2022.12.033
6. H. Ebrahimgol, M. Aghaie, A. Zolfaghari, A. Naserbegi, "A novel approach in exergy optimization of a WWER1000 nuclear power plant using whale optimization algorithm", *Ann. Nucl. Energy*, vol. 145, p. 107540, 2020. http://doi.org/10.1016/j.anucene.2020.107540
7. I. Maruyama *et al.*, “Radiation-induced alteration of sandstone concrete aggregate”, *J. Nucl. Mat.*, vol. 583, 154547, 2023. http://doi.org/10.1016/j.jnucmat.2023.154547

8. ICIC – International Committee on Irradiated Concrete. [Online]. Available: https://icic2023.ornl.gov [Accessed: Sep. 24, 2025].
9. T. Motta, A. Couet, R.J. Comstock, "Corrosion of zirconium alloys used for nuclear fuel cladding", *Annu. Rev. Mater. Res.*, vol. 45, pp. 311–343, 2015. http://doi.org/10.1146/annurev-matsci-070214-020951
10. S. Zhao, G. Ran, Y. Guo, Q. Han, S. Liu, F. Gao, "Study on the mechanism of helium platelets formation at low temperatures in SiC from the perspective of atomic diffusion", *J. Nucl. Mater.*, vol. 542, p. 152507, 2020. http://doi.org/10.1016/j.jnucmat.2020.152507
11. G. Van Rossum; F.L. Drake, *Python 3 Reference Manual*, CreateSpace, 2009.
12. M. Abadi et al., *TensorFlow: Large-Scale Machine Learning on Heterogeneous Systems*, 2015. arXiv:1603.04467
13. A. Leenaers et al., "Post-irradiation examination of AlFeNi cladded U_3Si_2 fuel plates irradiated under severe conditions", *J. Nucl. Mater.*, vol. 375, no. 2, pp. 243–251, 2008. http://doi.org/10.1016/j.jnucmat.2008.01.013
14. P. Mishra, V. Karthik, P.K. Shah, "Post Irradiation Examination of Fuel", in *Nuclear Fuel Cycle*, Springer, 2023, pp. 185–212. https://doi.org/10.1007/978-981-99-0949-0_6
15. J. Li, W. Xu, D. She, H. Xie, Z.-H. Liu, L. Shi, "Review of the development and application of high flux reactors", *Nucl. Sci. Tech.*, vol. 36, 227, 2025. https://doi.org/10.1007/s41365-025-01808-y
16. J.-W. Cho, Y. Choi, K. Jeong, J.-C. Shin, "Measurement of nuclear fuel rod deformation using an image processing technique", *Nucl. Eng. Technol.*, vol. 43, no. 2, pp. 133–139, 2011. http://doi.org/10.5516/NET.2011.43.2.133
17. F. Shadmehri, S.V. Hoa, "Digital Image Correlation Applications in Composite Automated Manufacturing, Inspection, and Testing", *Appl. Sci.*, vol. 9, no. 13, 2719, 2019. http://doi.org/10.3390/app9132719
18. P. Murray, G. West, S. Marshall, S. McArthur, "Automated in-core image generation from video to aid visual inspection of nuclear power plant cores", *Nucl. Eng. Des.*, vol. 300, pp. 57–66, 2016. http://doi.org/10.1016/j.nucengdes.2015.11.037
19. M. Devereux, P. Murray, G. West, S. Buckley-Mellor, G. Cocks, C. Lynch, A. Fletcher, "Automated analysis of AGR fuel channel inspection videos", presented at [Conf. 6th EDF-Energy Nuclear Graphite Conference], Kendal, UK, Oct. 2018. [Online]. Available: *[https://pure.strath.ac.uk/ws/portalfiles/portal/87986003/Devereux_etal_EDF_2018_Automated_analysis_of_AGR_fuel_channel_inspection.pdf]* [Accessed: Sep. 24, 2025]
20. J. Knotek, J. Blažek, M. Kopeć, "Simulating nuclear fuel inspections: Enhancing reliability through synthetic data", *Nucl. Eng. Technol.*, vol. 57, no. 8, 103571, 2025. http://doi.org/10.1016/j.net.2025.103571